Low Temperature Synthesis of Hierarchical TiO_2 Nanostructures for High Performance Perovskite Solar Cells by Pulsed Laser Deposition

Bin Yang,[†] *Masoud Mahjouri-Samani,*[†] *Christopher M. Rouleau,*

David B. Geohegan, Kai Xiao[*]

Center for Nanophase Materials Sciences, Oak Ridge National Laboratory, Oak Ridge, TN, 37831, USA.

*Correspondence to: xiaok@ornl.gov

[†] *These authors contributed equally to this work*

Notice: This manuscript has been authored by UT-Battelle, LLC, under Contract No. DE-AC05-00OR22725 with the U.S. Department of Energy. The United States Government retains and the publisher, by accepting the article for publication, acknowledges that the United States Government retains a non-exclusive, paid-up, irrevocable, world-wide license to publish or reproduce the published form of this manuscript, or allow others to do so, for United States Government purposes. The Department of Energy will provide public access to these results of federally sponsored research in accordance with the DOE Public Access Plan (http://energy.gov/downloads/doe-public-access-plan).

Low Temperature Synthesis of Hierarchical TiO_2 Nanostructures for High Performance Perovskite Solar Cells by Pulsed Laser Deposition

Bin Yang,[†] *Masoud Mahjouri-Samani,*[†] *Christopher M. Rouleau,*

David B. Geohegan, Kai Xiao[*]

Center for Nanophase Materials Sciences, Oak Ridge National Laboratory, Oak Ridge, TN, 37831, USA.

*Correspondence to: xiaok@ornl.gov

[†] *These authors contributed equally to this work*

Abstract

A promising way to advance perovskite solar cells is to improve the quality of the electron transport material – e.g., titanium dioxide (TiO_2) – in a direction that increases electron transport and extraction. Although dense TiO_2 films are easily grown in solution, efficient electron extraction suffers due to a lack of interfacial contact area with the perovskites. Conversely, mesoporous films do offer high surface-area-to-volume ratios, thereby promoting efficient electron extraction, but their morphology is relatively difficult to control via conventional solution synthesis methods. Here, a pulsed laser deposition method was used to assemble TiO_2 nanoparticles into TiO_2 hierarchical architectures exhibiting anatase crystal structure, and prototype solar cells employing these structures yielded power conversion efficiencies of ~ 14%. Our approach demonstrates a way to grow high aspect-ratio TiO_2 nanostructures for improved interfacial contact between TiO_2 and perovskite materials, leading to high electron-hole pair separation and electron extraction efficiencies for superior photovoltaic performance. Comparedto previous PLD-synthesized TiO_2 mesoporous crystalline networks that needed post-

thermal annealing at 500°C to form mesoporous crystalline networks, our relatively low temperature (300 ^{o}C) TiO_2 processing method may promote reduced energy-consumption during device fabrication as well as enable compatibility with flexible polymer substrates such as polyimide.

Keywords: Solar cells; Perovskite; TiO_2 nanostructures; Pulsed laser deposition

It is remarkable that in as little as seven years, organometallic halide perovskite solar cells[1-4] have been developed with certified power conversion efficiencies (PCE) of ~ 22%, a value that is comparable to existing thin film photovoltaic technologies based on, for example, copper indium gallium selenide and cadmium telluride.[5-8] To rival silicon based solar cells, however, tremendous effort has been focused on several critical matters in perovskite solar cells including exciton and carrier dynamics,[9-14] device operation mechanisms,[15-19] morphologic engineering,[20-23] synthesis and processing of new perovskite materials,[24-29] and electron or hole transport materials.[30, 31] Note that the light absorbing perovskite is usually sandwiched between hole transport and electron transport layers. Both are key factors to enable efficient separation of photogenerated electron-hole pairs and extraction of free electrons and holes for high performance perovskite-based cells. In these devices, the most common hole transport materials are conducting organic materials such as 2,2′,7,7′-tetrakis[N,N-di(p-methoxyphenylamine)]-9,9-spirobifluorene (Spiro-OMeTAD),[2, 3] Poly[bis(4-phenyl)(2,4,6-trimethylphenyl)amine] (PTAA),[32] and poly(3,4-ethylenedioxythiophene) polystyrene sulfonate (PEDOT:PSS).[16] Another category of hole transport materials is inorganics such as molybdenum oxide (MoO_x),[33] nickel oxide (NiO_X),[34] vanadium oxide (V_2O_5)[35], and tungsten trioxide (WO_3)[35]. We note that

inorganic films have been shown to perform better than organics in protecting the perovskite photoactive layer against ambient moisture induced degradation. For electron transport, the most widely used materials are fullerene derivatives[16] and titanium dioxide (TiO_2).[36] Titanium dioxide, in particular, is normally applied in two different ways: dense thin films or as a mesoporous scaffold.[2, 3] Dense TiO_2 films are readily grown in solution, but they suffers from the lack of sufficient interfacial contact area with the perovskites to ensure efficient electron extraction.[37] In contrast, mesoporous scaffolds have high surface-to-volume ratios and light-scattering abilities that can significantly trap light within the photoactive layer and further enhance the optical absorption for increased photogenerated currents; however its morphology is difficult to control via conventional solution synthesis methods such as sol-gel[38] or solvothermal synthesis.[38, 39]

Pulsed laser deposition (PLD) is a widely used technique for epitaxial oxide thin film growth, and typically results in the formation of dense and continuous films when performed in vacuum.[40] However, by spatial confinement of the ablation plume at relatively high background gas pressures, growth of nanoparticle assemblies in porous, hierarchical architectures can be achieved.[41-43] Such hierarchical TiO_2 nanostructures assembled at room temperature using PLD-synthesized TiO_2 nanoparticles can be post-annealed at 500°C to form mesoporous crystalline networks that have been used to achieve higher power conversion efficiencies in dye-sensitized solar cells (DSSCs), likely due to their larger surface area and stronger light scattering.[44, 45, 46] These PLD-grown, post-annealed, three-dimensional TiO_2 nanostructures have also been shown be good electron acceptors and transporters that have the potential to enhance exciton dissociation and photogenerated charge collection in high efficiency poly(3-hexylthiophene) (P3HT)/TiO_2 solar cells.[47] However, in spite of this effort in applying TiO_2 nanostructures in

dye-sensitized and polymer solar cells, the use of PLD-synthesized TiO_2 nanostructures in organometallic halide perovskite solar cells is still poorly studied.

Here, we report the PLD growth of hierarchical TiO_2 films at relatively low (300°C) substrate temperatures to enable the single-step fabrication of electrodes for high-efficiency perovskite solar cells that combine the advantages of both dense thin films and mesoporous scaffolds. The final structures exhibited high aspect-ratios, mesoporosity, and a crystalline phase that was predominantly anatase. Although significantly denser than the architectures deposited at room temperature, such TiO_2 nanostructures were still porous, enabling rapid infiltration of the perovskite precursor solution. A prototype photovoltaic device yielded a PCE of 14%, demonstrating great promise for further photovoltaic applications.

To grow TiO_2 nanostructures by PLD, a 248 nm laser beam was used to ablate a TiO_2 target to deposit TiO_2 nanoparticles (~ 3-5 nm) in 200 mT of oxygen,[48] onto an ITO glass substrate positioned 5 cm away. As illustrated in **Figure 1a**, the nanoparticle assemblies form a hierarchical TiO_2 nanostructure. **Figure 1b** and **1c** exhibit surface and cross-sectional scanning electron microscopy (SEM) images of TiO_2 nanostructures on a silicon substrate grown by this method at room temperature, showing a hierarchical nanostructure. The phase, structure, and degree of crystallinity were readily controlled by tuning the temperature of indium tin oxide (ITO) glass substrates on the heater stage. **Figure 1d** and **1e** shows surface and cross-sectional morphologies of a PLD grown TiO_2 film at 300 ^{o}C, respectively. Such TiO_2 films are relatively porous as a result of the assembly of ~3-5 nm size nanoparticles as demonstrated in our previous work.[48] These pores allow the liquid perovskite precursors to diffuse into the TiO_2 nanostructures for excellent interfacial contact between the nanoparticles and perovskites. Note that the use of low temperature (300 ^{o}C) induced crystallization of the TiO_2 nanoparticles during deposition, but

prevented the structure from forming a fully dense film, hence enabling both porosity and crystallinity. The degree of crystallinity, phase, and nanostructured morphology are function of deposition conditions, and will be the subject of a separate publication.

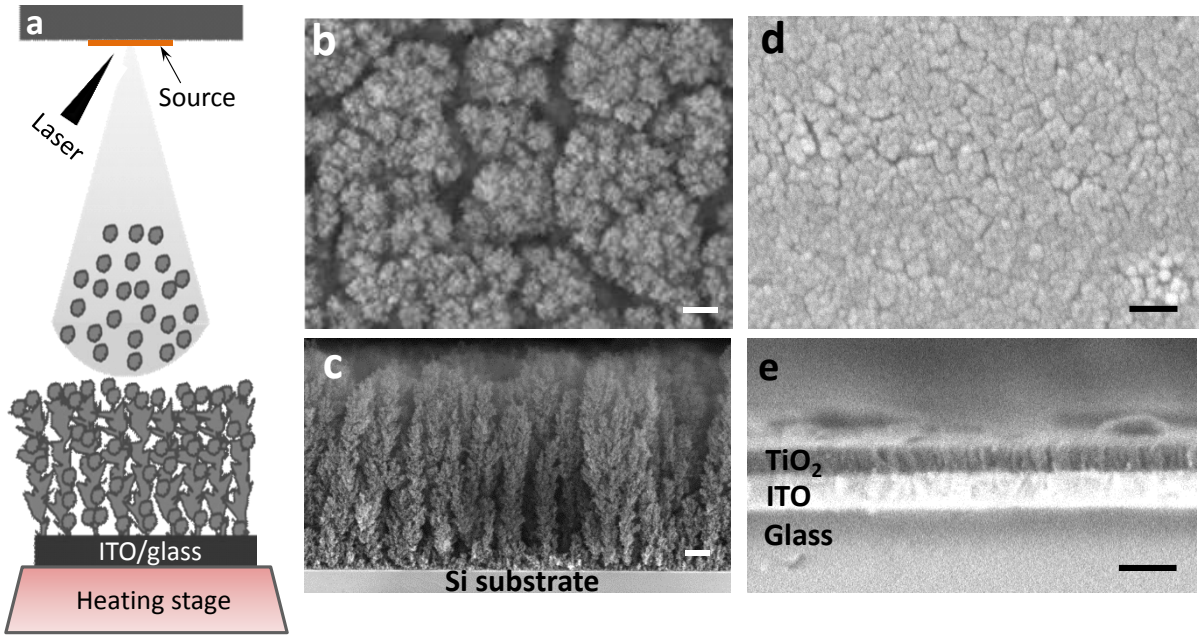

Figure 1. Growth of TiO_2 nanoarchitectures by pulsed laser deposition: (a) Schematic plot to show the growth process of TiO_2 on a heated ITO glass substrateSurface (b) and cross-sectional (c) SEM image of the TiO_2 architecture of assembled 3-5 nm nanoparticles deposited on a silicon substrate by PLD at room temperature. Surface (d) and cross-sectional (e) SEM image of the TiO_2 nanostructure deposited on an ITO glass substrate by PLD under similar conditions, but at 300 ^{o}C. The scale bar in (b-e) is 200 nm.

X-ray diffraction (XRD) and Raman spectroscopy measurements were applied to examine the crystallinity of the PLD-deposited TiO_2 films. As shown by XRD the patterns in **Figure 2a**, the unannealed TiO_2 structures showed amorphous characteristics, whereas the samples grown at higher substrate temperatures (300 °C) exhibited the onset of crystalline features of the anatase phase, as suggested by the appearance of a reflex at ~ 25°. Raman spectroscopy studies further confirmed that the crystalline phase was anatase as evidenced by characteristic Raman peaks at ~144, 399, and 639 cm^{-1}.[49] We note that our experiments showed that a deposition temperature

of 300 °C was sufficient to form anatase during PLD, and is *much* lower than that (500 °C) required for conventional solution-processed TiO_2 thin films[18, 36, 50, 51] and post-thermal annealing temperature of 500 °C needed for the formation of previous PLD-synthesized TiO_2 mesoporous crystalline networks.[44,45,46] Interestingly, our relatively low temperature TiO_2 processing method may enable reduced energy consumption during fabrication of perovskite photovoltaics as well as pave the way for use of flexible polymer substrates such as polyimide.[52] Note that the rutile and brookite phases of TiO_2 are also able to synthesize by our PLD method,[48] but this requires much higher growth temperature (> 500 °C) which would degrade the ITO glass substrates due to elemental diffusion at such high temperatures to degrade optical and electronic properties,[53, 54] and also induce to sinter our ~ 3 nm nanoparticles to large size particles (~ 15-50 nm) resulting in the reduction of surface area. [48]

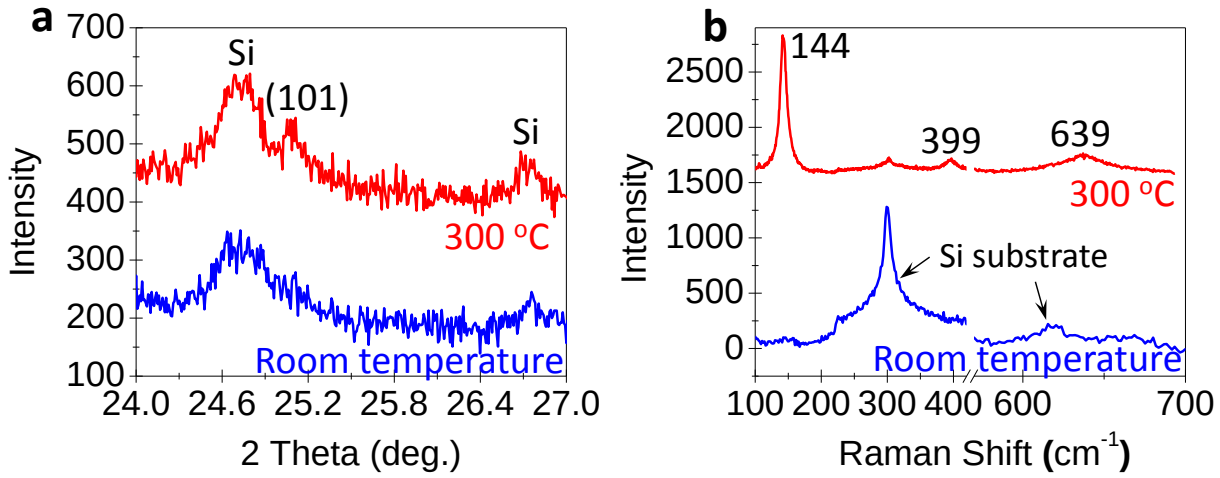

Figure 2. Crystallinity of TiO_2 films. XRD pattern (a) and Raman spectra (b) acquired from TiO_2 film grown on a silicon substrate at room temperature (blue) and 300 °C (red). Both methods indicate the formation of anatase structure when the substrate temperature was 300 °C.

To test the suitability of the porous, semicrystalline TiO_2 nanostructured films deposited at 300°C as an electron transporter in perovskite solar cells, we fabricated prototype solar cells using our previously established layer-by-layer processing method, whereby precursor inks were

deposited followed by a room-temperature-air-exposure treatment.[36] Specifically, a lead(II) iodide (PbI_2) solution with a concentration of 550 mg/mL was dropped onto TiO_2 layers, and in order to infiltrate the PbI_2 solution into the porous region of the TiO_2 layer, we waited ~5 seconds before spin-coating to remove excess material. After that, CH_3NH_3I (70 mg/mL) was spin-coated, and then the device was left under ambient condition for an hour. Our previous study has demonstrated that ambient air exposure can sufficiently drive the interdiffusion between PbI_2 and CH_3NH_3I layers to form perovskites after 1 hour.[36] As indicated by the disappearance of the (001), (100), and (002) PbI_2 reflexes and the appearance of the (110), (112), and (202) $CH_3NH_3PbI_3$ reflexes, XRD confirmed complete transformation of the PbI_2 precursor to $CH_3NH_3PbI_3$ perovskite after 1 hour (**Figure 3**).

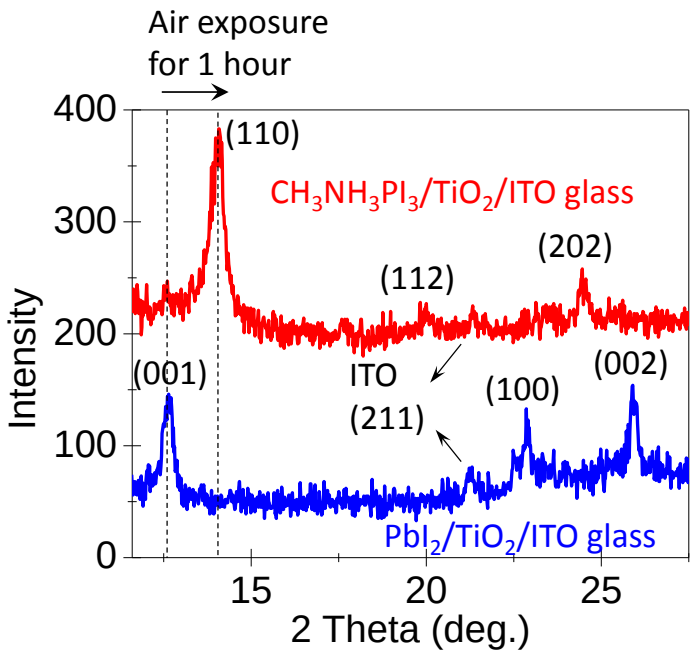

Figure 3. X-ray diffraction pattern of the original PbI_2/TiO_2/ITO glass sample (blue) and final $CH_3NH_3PbI_3/TiO_2$/ITO glass sample (red) after 1 hour. The sample was made by spin-coating CH_3NH_3I solution onto the original PbI_2/TiO_2/ITO glass sample, and then exposing to air for 1 hour.

In order to inspect whether the $CH_3NH_3PbI_3$ perovskite diffused into the pores of the TiO_2, cross-sectional SEM images and associated energy dispersive X-ray spectroscopy (EDS) maps were acquired as shown in **Figure 4**. In particular, the TiO_2 nanostructures were observed to be ~150 nm tall, and supported a $CH_3NH_3PbI_3$ perovskite layer that was ~250 nm thick. To determine if the perovskite infiltrated the TiO_2 nanstructure, EDS maps were acquired as shown in **Figure 4b**. It should be noted that the low resolution and contrast of the SEM image shown in **Figure 4b-i** are due to charging caused by the 20 kV accelerating voltage used for EDS. We acquired EDS maps (**Figure 4b**) for iodine (I), lead (Pb), titanium (Ti), and indium (In), and ascribed the images to the perovskite, TiO_2, and ITO, respectively. The distribution region of In matches well with the ITO layer shown in **Figures 4b-i and v**. The TiO_2 layer as indicated by the distribution of Ti (**Figure 4b-iv**) is above the ITO layer, and more importantly, it appears that the distribution of Ti overlaps with the bottom part of the distribution of I and Pb (**Figure 4b-ii** and **4b-iii**), suggesting the $CH_3NH_3PbI_3$ perovskite diffused into the TiO_2 nanostructure. An EDS spectrum was also taken in the rectangular region as indicated in **Figure 4b-I**, and the strong signals of Ti, O, Pb, and I further confirm that the $CH_3NH_3PbI_3$ perovskite is intermixed with the TiO_2.

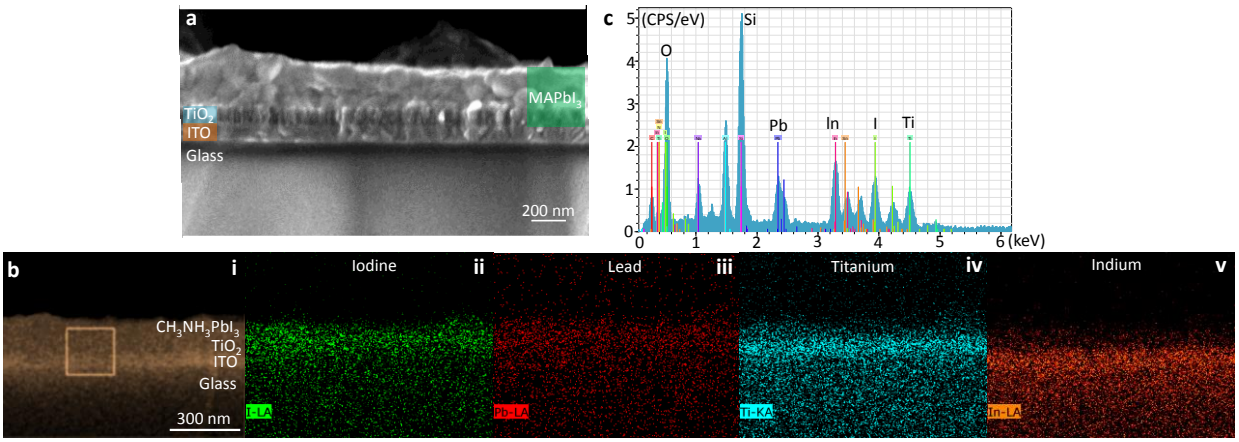

Figure 4. (a) Cross-sectional morphology of an ITO glass/TiO_2/$CH_3NH_3PbI_3$ perovskite sample. (b-c) Energy dispersive X-ray spectroscopy analysis: (b-i) SEM image and corresponding EDS images for iodine (b-ii), lead (b-iii), titanium (b-iv), and indium (b-v); (c) EDS spectrum acquired in the square region as indicated in (b-i).

A series of TiO_2 nanostructures with different thicknesses were used to make perovskite solar cells to study the effect of TiO_2 thickness on cell efficiency, and their performance is shown in **Figure 5**. The devices did exhibit hysteresis (**Figure 5a**), making the PCE at forward to reverse bias, 13.6%, while that from reverse to forward bias, only 8.9%. In order to stabilize our devices and mitigate this effect, we soaked them under an illumination of 100 mW/cm^2 at 1 V bias for 30 seconds. As shown in **Figure 5b**, the *J-V* curves showed little change for four individual scans after soaking, and allowed us to accurately compare the devices with different TiO_2 thicknesses. The origin of *J-V* hysteresis in our devices may be owing to: i) I^- or $CH_3NH_3^+$ ionic migration in perovskites[55, 56] and ii) charge trapping/de-trapping at surface trap states of the perovskites.[57, 58] The devices were stabilized by illuminating the device at bias of 1 V because the injected charges could fill up the trap states in perovskites.[57, 59] Interestingly, devices based on 150 nm thick TiO_2 showed a short circuit current density (J_{SC}) of 20.1 mA/cm^2, open circuit voltage (V_{OC}) of 1.01 V, fill factor (*FF*) of 69%, and PCE of 14.1%. By increasing the thickness of the TiO_2 layer to 200 nm, the photovoltaic performance showed little change. At to 400 nm, however, the PCE decreased by about 20%, primarily due to reduced V_{OC} and *FF*. It should be pointed out that the decrease in both V_{OC} and *FF* in the case of the thickest TiO_2 is either likely due to the increased series resistance in the TiO_2 electron transport layer or the direct contact of TiO_2 with Spiro-OMeTAD. Based upon the TiO_2 thickness dependence of device performance shown here, further improvement in PCE can be expected by optimizing the TiO_2 nanostructure and morphology.

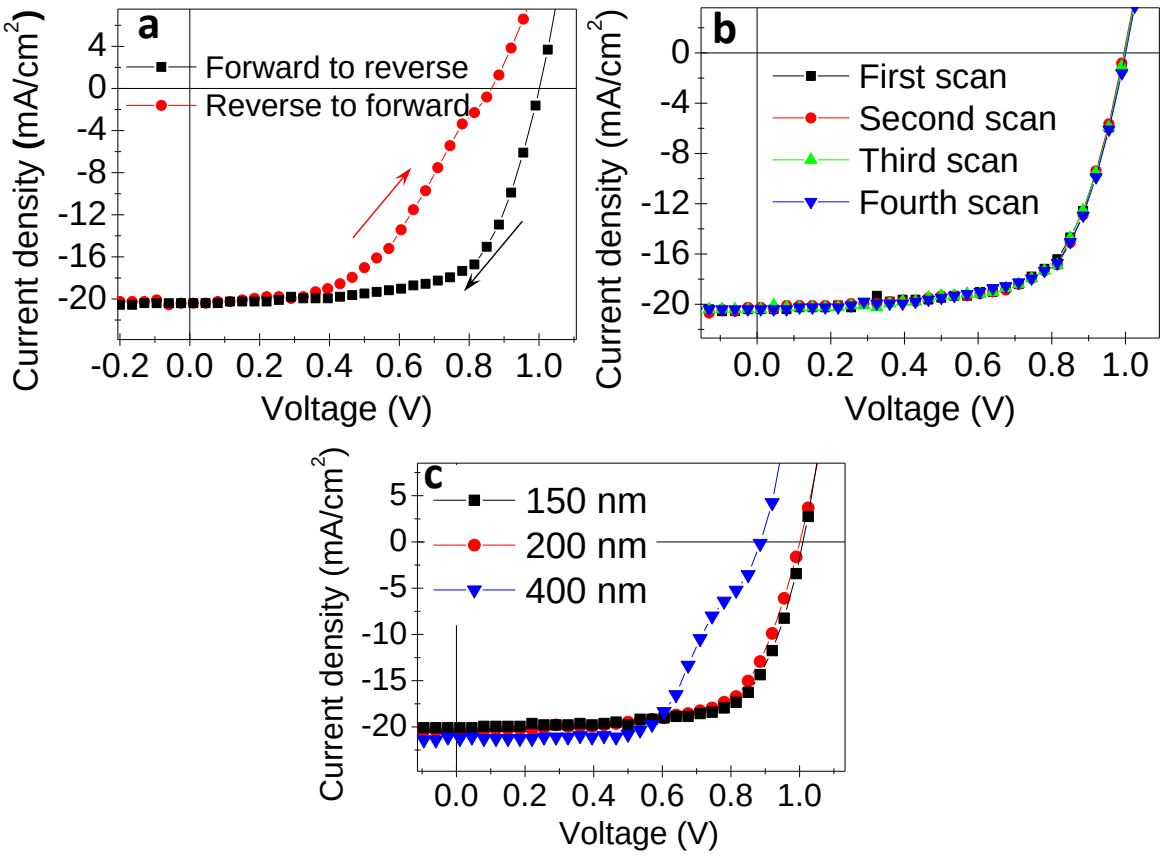

Figure 5. Photovoltaic performance (*J-V* curves) of perovskite devices. (a) Hysteresis of *J-V* curves acquired from scanning from forward bias to reverse bias and then from reverse bias to forward bias. (b) *J-V* curves with multiple scans after illumination soaking process showing negligible difference. (c) *J-V* curve of the devices with different TiO_2 thicknesses.

In conclusion, mesoporous TiO_2 nanostructures grown by pulsed laser deposition at low substrate temperatures of 300°C were explored as electron transport layers in perovskite solar cells, and were found to yield a PCE of ~14%. The semicrystalline anatase TiO_2 nanoparticle assembled nanostructures were found to have high surface area, thus ensuring high interfacial contact between the TiO_2 and perovskite, and leading to high photovoltaic performance that was likely due to high exciton dissociation and charge extraction efficiencies. It is expected that the further study on optimizing the TiO_2 nanostructure and morphology may further enhance the

device performance of perovskite solar cells beyond what was reported here. Compared to previous PLD-synthesized TiO_2 mesoporous crystalline networks that needed post-thermal annealing at 500°C to form mesoporous crystalline networks,[44,45,46] our relatively low temperature (300 ^{o}C) TiO_2 processing method may not only enable the reduce energy consumption during the perovskite photovoltaic fabrication process, but offers compatibility with flexible polymer substrates such as polyimide.

Experimental section

Pulsed laser deposition

KrF-laser (248 nm) ablation of the TiO_2 target with laser fluence of 1 J cm^{-2} and repetition rate of 2 Hz in 200 mT of oxygen background gas pressure was used to synthesize the desired structures. ITO glass substrates were mounted onto a 1 inch button heater and heated to 300 ^{o}C suitable for the formation of anatase structures. The target to substrate distance was set to insure the plume tip just slightly reaches the surface of the substrate, a condition suitable for the growth of these structures. Different thicknesses of TiO_2 were prepared by the number of laser pulses.

Thin film characterization

A Renishaw Raman spectroscopy system (532 nm excitation source focused onto the samples through a 50X 0.8 NA objective lens) was used to characterize the samples. An X-ray diffractometer (Panalytical X'Pert MPD Pro) with Cu-Kα radiation (λ=1.54050Å) was used to acquire XRD patterns. A scanning electron microscope (Zeiss Merlin) was used to acquire the SEM images. Accelerating voltages of 5 kV and 3 kV were used to acquire surface and cross-sectional SEM images respectively. An accelerating voltage of 20 kV was applied to take the EDS imaging with a sample stage tilt angle of 15°.

Device fabrication and characterization

The TiO_2 nanostructures were grown on precleaned ITO glass substrates. The 550 mg/mL PbI_2 solution (use dimethylformamide as a solvent) was then dropped onto TiO_2 films. After waiting for 5 seconds to allow the PbI_2 solution to diffuse into TiO_2 nanostructures, the sample was spin-coated at 6000 rpm to remove excess PbI_2. CH_3NH_3I solution (72 mg/mL, 2-propanol used as a solvent) was subsequently spin-coated onto the PbI_2. The samples were then placed in ambient air for 1 hour to ensure the PbI_2 precursor transformed into the $CH_3NH_3PbI_3$ perovskite. Spiro-OMeTAD solution (90 mg/mL, chlorobenzene used as a solvent) was spin-coated at 2000 rpm, and then kept in a desiccator overnight. Finally, a 100 nm-thick silver film was evaporated with a rate of 1 Å/s. The active area was ~ 6.5 mm^2, which was determined by an optical microscopy. The *J-V* curves were collected under illumination (100 mW/cm^2, AM 1.5 G solar spectrum, (Radiant Source Technology, 300 W, Class A) using a Keithley 2400 source meter. The light intensity was calibrated using a NIST-certified Si-reference cell. The *J-V* curves were obtained by scanning from forward bias to reverse bias and then from reverse bias to forward bias, with a 50 ms sweep delay time. Prior to measurements, the devices were soaked under illumination (100 mW/cm^2) at a voltage bias of ~1 V for 30 seconds to stabilize the photovoltaic performance. The measurements were conducted in a N_2-filled glovebox.

Acknowledgement

Synthesis of TiO_2 nanostructures sponsored by the Materials Science and Engineering Division, Office of Basic Energy Sciences, U.S. Department of Energy. Photovoltaic device fabrication and characterization were conducted at the Center for Nanophase Materials Sciences (CNMS), which is a DOE Office of Science User Facility. We thank Dale Hensley for the assistance in acquiring EDS maps.

Competing financial interests

The authors declare no competing financial interests.

Reference

1. Kojima, A.; Teshima, K.; Shirai, Y.; Miyasaka, T. *J. Am. Chem. Soc.* **2009,** *131*, 6050-6051.
2. Liu, M.; Johnston, M. B.; Snaith, H. J. *Nature* **2013,** *501*, 395-398.
3. Burschka, J.; Pellet, N.; Moon, S.-J.; Humphry-Baker, R.; Gao, P.; Nazeeruddin, M. K.; Grätzel, M. *Nature* **2013,** *499*, 316-319.
4. Im, J.-H.; Lee, C.-R.; Lee, J.-W.; Park, S.-W.; Park, N.-G. *Nanoscale* **2011,** *3*, 4088-4093.
5. Bi, D.; Tress, W.; Dar, M. I.; Gao, P.; Luo, J.; Renevier, C.; Schenk, K.; Abate, A.; Giordano, F.; Baena, J.-P. C. *Sci. Adv.* **2016,** *2*, e1501170.
6. Jeon, N. J.; Noh, J. H.; Yang, W. S.; Kim, Y. C.; Ryu, S.; Seo, J.; Seok, S. I. *Nature* **2015,** *517*, 476-480.
7. Yang, W. S.; Noh, J. H.; Jeon, N. J.; Kim, Y. C.; Ryu, S.; Seo, J.; Seok, S. I. *Science* **2015,** *348*, 1234-1237.
8. *http://www.nrel.gov/ncpv/images/efficiency_chart.jpg* **NREL efficiency chart. ,** *(accessed April 2016)*.
9. Simpson, M. J.; Doughty, B.; Yang, B.; Xiao, K.; Ma, Y.-Z. *J. Phys. Chem. Lett.* **2015,** *6*, 3041-3047.
10. Watson, B. R.; Yang, B.; Xiao, K.; Ma, Y.-Z.; Doughty, B.; Calhoun, T. R. *J. Phys. Chem. Lett.* **2015,** *6*, 3283-3288.
11. Manser, J. S.; Kamat, P. V. *Nature Photon.* **2014,** *8*, 737-743.
12. Doughty, B.; Simpson, M. J.; Yang, B.; Xiao, K.; Ma, Y.-Z. *Nanotechnology* **2016,** *27*, 114002.
13. Simpson, M. J.; Doughty, B.; Yang, B.; Xiao, K.; Ma, Y.-Z. *ACS Photonics* **2016,** *3*, 434-442.
14. Frost, J. M.; Butler, K. T.; Brivio, F.; Hendon, C. H.; Van Schilfgaarde, M.; Walsh, A. *Nano Lett.* **2014,** *14*, 2584-2590.
15. de Quilettes, D. W.; Vorpahl, S. M.; Stranks, S. D.; Nagaoka, H.; Eperon, G. E.; Ziffer, M. E.; Snaith, H. J.; Ginger, D. S. *Science* **2015,** *348*, 683-686.
16. Shao, Y.; Xiao, Z.; Bi, C.; Yuan, Y.; Huang, J. *Nat. Commun.* **2014,** *5*, 5784.
17. Xing, G.; Mathews, N.; Sun, S.; Lim, S. S.; Lam, Y. M.; Grätzel, M.; Mhaisalkar, S.; Sum, T. C. *Science* **2013,** *342*, 344-347.
18. Yang, B.; Dyck, O.; Poplawsky, J.; Keum, J.; Puretzky, A.; Das, S.; Ivanov, I.; Rouleau, C.; Duscher, G.; Geohegan, D. *J. Am. Chem. Soc.* **2015,** *137*, 9210-9213.
19. Gottesman, R.; Haltzi, E.; Gouda, L.; Tirosh, S.; Bouhadana, Y.; Zaban, A.; Mosconi, E.; De Angelis, F. *J. Phys. Chem. Lett.* **2014,** *5*, 2662-2669.
20. Zhou, Y.; Yang, M.; Wu, W.; Vasiliev, A. L.; Zhu, K.; Padture, N. P. *J. Mater. Chem. A* **2015,** *3*, 8178-8184.
21. Liang, P. W.; Liao, C. Y.; Chueh, C. C.; Zuo, F.; Williams, S. T.; Xin, X. K.; Lin, J.; Jen, A. K. Y. *Adv. Mater.* **2014,** *26*, 3748-3754.
22. Nie, W.; Tsai, H.; Asadpour, R.; Blancon, J.-C.; Neukirch, A. J.; Gupta, G.; Crochet, J. J.; Chhowalla, M.; Tretiak, S.; Alam, M. A. *Science* **2015,** *347*, 522-525.
23. Bi, C.; Wang, Q.; Shao, Y.; Yuan, Y.; Xiao, Z.; Huang, J. *Nat. Commun.* **2015,** *6*, 7747.
24. Eperon, G. E.; Stranks, S. D.; Menelaou, C.; Johnston, M. B.; Herz, L. M.; Snaith, H. J. *Energy Environ. Sci.* **2014,** *7*, 982-988.

25. Hao, F.; Stoumpos, C. C.; Cao, D. H.; Chang, R. P. H.; Kanatzidis, M. G. *Nature Photon.* **2014,** *8*, 489-494.
26. Lin, Q.; Armin, A.; Nagiri, R. C. R.; Burn, P. L.; Meredith, P. *Nature Photon.* **2015,** *9*, 106-112.
27. Yang, B.; Keum, J.; Ovchinnikova, O. S.; Belianinov, A.; Chen, S.; Du, M.-H.; Ivanov, I. N.; Rouleau, C. M.; Geohegan, D. B.; Xiao, K. *J. Am. Chem. Soc.* **2016,** *138*, 5028–5035.
28. Rong, Y.; Tang, Z.; Zhao, Y.; Zhong, X.; Venkatesan, S.; Graham, H.; Patton, M.; Jing, Y.; Guloy, A. M.; Yao, Y. *Nanoscale* **2015,** *7*, 10595-10599.
29. Hao, F.; Stoumpos, C. C.; Cao, D. H.; Chang, R. P.; Kanatzidis, M. G. *Nature Photon.* **2014,** *8*, 489-494.
30. Zhou, H.; Chen, Q.; Li, G.; Luo, S.; Song, T.-b.; Duan, H.-S.; Hong, Z.; You, J.; Liu, Y.; Yang, Y. *Science* **2014,** *345*, 542-546.
31. Sun, K.; Chang, J.; Isikgor, F. H.; Li, P.; Ouyang, J. *Nanoscale* **2015,** *7*, 896-900.
32. Yang, W. S.; Noh, J. H.; Jeon, N. J.; Kim, Y. C.; Ryu, S.; Seo, J.; Seok, S. I. *Science* **2015,** *348*, 1234-1237.
33. Zhao, Y.; Nardes, A. M.; Zhu, K. *Appl. Phys. Lett.* **2014,** *104*, 213906.
34. Jeng, J. Y.; Chen, K. C.; Chiang, T. Y.; Lin, P. Y.; Tsai, T. D.; Chang, Y. C.; Guo, T. F.; Chen, P.; Wen, T. C.; Hsu, Y. J. *Adv. Mater.* **2014,** *26*, 4107-4113.
35. Meng, L.; You, J.; Guo, T.-F.; Yang, Y. *Acc. Chem. Res.* **2015**.
36. Yang, B.; Dyck, O.; Poplawsky, J.; Keum, J.; Das, S.; Puretzky, A.; Aytug, T.; Joshi, P. C.; Rouleau, C. M.; Duscher, G. *Angew. Chem. Int. Ed.* **2015,** *54*, 14862-14865.
37. Grätzel, M. *Nature Mater.* **2014,** *13*, 838-842.
38. Chen, D.; Huang, F.; Cheng, Y. B.; Caruso, R. A. *Adv. Mater.* **2009,** *21*, 2206-2210.
39. Chen, D.; Cao, L.; Huang, F.; Imperia, P.; Cheng, Y.-B.; Caruso, R. A. *J. Am. Chem. Soc.* **2010,** *132*, 4438-4444.
40. Lowndes, D. H.; Geohegan, D.; Puretzky, A.; Norton, D.; Rouleau, C. *Science* **1996,** *273*, 898-903.
41. Geohegan, D.; Puretzky, A.; Rader, D. *Appl. Phys. Lett.* **1999,** *74*, 3788-3790.
42. Mahjouri‐Samani, M.; Gresback, R.; Tian, M.; Wang, K.; Puretzky, A. A.; Rouleau, C. M.; Eres, G.; Ivanov, I. N.; Xiao, K.; McGuire, M. A. *Adv. Funct. Mater.* **2014,** *24*, 6365-6371.
43. Geohegan, D. B.; Puretzky, A. A.; Duscher, G.; Pennycook, S. J. *Appl. Phys. Lett.* **1998,** *72*.
44. Weng, Z.; Guo, H.; Liu, X.; Wu, S.; Yeung, K.; Chu, P. K. *RSC Adv.* **2013,** *3*, 24758-24775.
45. Passoni, L.; Ghods, F.; Docampo, P.; Abrusci, A.; Martí-Rujas, J.; Ghidelli, M.; Divitini, G.; Ducati, C.; Binda, M.; Guarnera, S. *ACS Nano* **2013,** *7*, 10023-10031.
46. Sauvage, F.; Di Fonzo, F.; Li Bassi, A.; Casari, C.; Russo, V.; Divitini, G.; Ducati, C.; Bottani, C.; Comte, P.; Graetzel, M. *Nano Lett.* **2010,** *10*, 2562-2567.
47. Ghadirzadeh, A.; Passoni, L.; Grancini, G.; Terraneo, G.; Li Bassi, A.; Petrozza, A.; Di Fonzo, F. *ACS Appl. Mater. Interfaces* **2015,** *7*, 7451-7455.
48. Tian, M.; Mahjouri-Samani, M.; Eres, G.; Sachan, R.; Yoon, M.; Chisholm, M. F.; Wang, K.; Puretzky, A. A.; Rouleau, C. M.; Geohegan, D. B. *ACS Nano* **2015,** *9*, 10482-10488.
49. Ohsaka, T.; Izumi, F.; Fujiki, Y. *J. Raman spectrosc.* **1978,** *7*, 321-324.
50. Docampo, P.; Ball, J. M.; Darwich, M.; Eperon, G. E.; Snaith, H. J. *Nat. Commun.* **2013,** *4*, 2761.

51. Das, S.; Yang, B.; Gu, G.; Joshi, P. C.; Ivanov, I. N.; Rouleau, C. M.; Aytug, T.; Geohegan, D. B.; Xiao, K. *ACS Photonics* **2015,** *2*, 680-686.
52. Ok, K.-H.; Kim, J.; Park, S.-R.; Kim, Y.; Lee, C.-J.; Hong, S.-J.; Kwak, M.-G.; Kim, N.; Han, C. J.; Kim, J.-W. *Sci. Rep.* **2015,** *5*, 9464
53. Boyadzhiev, S. I.; Rassovska, M. M.; Matsumura, Y.; Kotani, Y.; Yordanov, R. S.; Yordanova, I. R. In *Characterization of reactive sputtered ITO and TiO 2/ITO thin films for applications at elevated temperatures*, Electronics Technology (ISSE), 2010 33rd International Spring Seminar on, IEEE: 2010; pp 65-70.
54. Lampert, C. M. *Sol. Energy Mater.* **1981,** *6*, 1-41.
55. Yuan, Y.; Huang, J. *Acc. Chem. Res.* **2016,** *49*, 286-293.
56. Eames, C.; Frost, J. M.; Barnes, P. R.; O'regan, B. C.; Walsh, A.; Islam, M. S. *Nature Commun.* **2015,** *6*, 7497.
57. Shao, Y.; Xiao, Z.; Bi, C.; Yuan, Y.; Huang, J. *Nature Commun.* **2014,** *5*, 5784.
58. Snaith, H. J.; Abate, A.; Ball, J. M.; Eperon, G. E.; Leijtens, T.; Noel, N. K.; Stranks, S. D.; Wang, J. T.-W.; Wojciechowski, K.; Zhang, W. *J. Phys. Chem. Lett.* **2014,** *5*, 1511-1515.
59. Wu, B.; Fu, K.; Yantara, N.; Xing, G.; Sun, S.; Sum, T. C.; Mathews, N. *Adv. Energy Mater.* **2015,** *5*, 1500829.

Table of Contents Entry

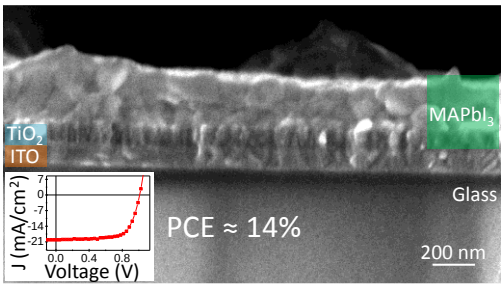

High aspect-ratio TiO_2 nanostructures directly assembled with pulsed laser deposition could improve interfacial contact for superior perovskite photovoltaic cells.